



RESEARCH ARTICLE

10.1002/2014JC010381

Characterizing horizontal variability and energy spectra in the Arctic Ocean halocline

Charlotte L. J. Marcinko¹, Adrian P. Martin¹, and John T. Allen²¹National Oceanography Centre, European Way, Southampton, UK, ²School of Earth and Environmental Sciences, University of Portsmouth, Portsmouth, Hampshire, UK

Key Points:

- Arctic energy spectra are steeper than those from midlatitude open oceans
- Energy variance is $O(100)$ less in perennial compared to marginal sea-ice
- Spectra suggest similar physical dynamics in perennial and marginal ice

Correspondence to:

C. L. J. Marcinko,
c.marcinko@noc.ac.uk

Citation:

Marcinko, C. L. J., A. P. Martin, and J. T. Allen (2015), Characterizing horizontal variability and energy spectra in the Arctic Ocean halocline, *J. Geophys. Res. Oceans*, 120, 436–450, doi:10.1002/2014JC010381.

Received 11 AUG 2014

Accepted 3 JAN 2015

Accepted article online 8 JAN 2015

Published online 28 JAN 2015

Abstract Energy transfer from the atmosphere into the upper Arctic Ocean is expected to become more efficient as summer sea-ice coverage decreases and multiyear ice thins due to recent atmospheric warming. However, relatively little is known about how energy is transferred within the ocean by turbulent processes from large to small scales in the presence of ice and how these pathways might change in future. This study characterizes horizontal variability in several regions of the Eurasian Arctic Ocean under differing sea-ice conditions. Historic along track CTD data collected by a Royal Navy submarine during summer 1996 allow a unique examination of horizontal variability and associated wavenumber spectra within the Arctic Ocean halocline. Spectral analysis indicates that potential energy variance under perennial sea-ice in the Amundsen Basin is $O(100)$ less than within the marginal ice zone (MIZ) of Fram Strait. Spectra from all regions show a transition in scaling at wavelengths of approximately 5–7 km. At scales greater than the transition wavelength to 50 km, energy spectra are consistent with a k^{-3} scaling (where k is a wavenumber) and interior quasigeostrophic dynamics. The scaling of spectra at these scales is extremely similar between regions suggesting similar dynamics and energy exchange pathways. The k^{-3} scaling is steeper than typically found in regions of midlatitude open ocean. At scales below the transition wavelength to 300 m, spectra are close to a $k^{-5/3}$ scaling or flatter, indicating a change in dynamics, which is potentially due to internal waves dominating variability at small scales.

1. Introduction

Atmospheric temperatures across the Arctic have, in recent years, been rising at approximately twice the rate of the Northern Hemisphere as a whole [Serreze and Barry, 2011]. This warming has led to significant thinning of multiyear sea-ice in the central Arctic Ocean and dramatic decreases in summer ice extent [Comiso et al., 2008; Kwok et al., 2009]. An ice-free summer is predicted within the next few decades [Wang and Overland, 2009]. As summer sea-ice extent decreases and the ice pack loosens, energy transfer from the atmosphere into the upper Arctic Ocean is expected to become more efficient. It is hypothesized that as wind begins to act directly on the ocean surface inertial motions and the internal wave field will strengthen [Guthrie et al., 2013]. Mesoscale activity may also increase as fronts and currents become more strongly forced [Rainville et al., 2011]. Such increases in upper ocean turbulence have the potential to significantly enhance mixing and modify water column stratification, changing the properties and dynamics of the Arctic Ocean [Rainville and Winsor, 2008].

Turbulent processes within the ocean are responsible for transferring variance in velocity, heat, and salinity generated at the basin scale through eight orders of magnitude to the dissipation scale $O(0.01)$ m [Müller et al., 2005]. Currently, relatively little is known regarding the transfer of these properties and energy by turbulent processes across the mesoscale to smaller scales. This is especially true in the presence of sea-ice where additional dynamic and thermodynamic processes such as ice-ocean shear, ice formation, and brine rejection take place. Understanding ocean turbulence, the pathways of energy exchange and how they may differ between ice-covered and ice-free oceans is important to ensure mesoscale and smaller scale turbulent processes can be correctly parameterized within regional and global models for accurate predictions of future climate. Dynamics may not only vary between ice-covered and ice-free oceans but also with sea-ice concentration, as marginal ice zones (MIZ) are often areas of maximum wind stress due to the roughness of broken ice and are associated with wind-driven Ekman convergence or divergence along the ice edge [Rainville et al., 2011]. Here we investigate horizontal variability and associated potential energy wavenumber spectra within the Eurasian Arctic Ocean MIZ and perennial sea-ice to assess if and how dynamics differ within regions of varying sea-ice cover and from regions of open ocean.

This is an open access article under the terms of the Creative Commons Attribution License, which permits use, distribution and reproduction in any medium, provided the original work is properly cited.

Wavenumber spectra of dynamical quantities in the upper ocean are typically characterized by a k^{-m} power law where k is a wavenumber and m characterizes the distribution of the quantity examined across wavelength scales. The larger m , the greater the variability at large scales relative to small scales. Observations from regions of midlatitude open ocean have frequently indicated a k^{-2} scaling of horizontal energy wavenumber spectra within the mixed layer and thermocline. Within the North Pacific, *Samelson and Paulson* [1988] found k^{-2} scaling of potential energy spectra at wavelengths of $O(1)$ to $O(100)$ km in the thermocline and within the mixed layer between scales of $O(10)$ to $O(100)$ km. Later studies within the North Pacific confirmed the k^{-2} scaling within the mixed layer and the thermocline at wavelengths from $O(1)$ to $O(100)$ km [*Ferrari and Rudnick*, 2000] and wavelengths of 30–400 km [*Cole et al.*, 2010]. Similar results have also been reported for the North Atlantic [*Katz*, 1975]. These observations are in agreement with high resolution numerical simulations which show a k^{-2} scaling for the upper ocean across a wavelength range of $O(1)$ to $O(100)$ km [*Capet et al.*, 2008b; *Klein et al.*, 2008]. This scaling is said to be consistent with surface quasigeostrophic dynamics [*Blumen*, 1978]. Model simulations indicate potential energy spectra only scale more steeply, between k^{-3} and k^{-4} , below the thermocline at depth (>800 m) where small scales are much less energetic and interior quasigeostrophic dynamics dominate. However, a k^{-3} scaling of energy spectra were previously found from observations in the mixed layer of the North Pacific at wavelengths of 1–10 km [*Samelson and Paulson*, 1988] and the Atlantic Gulf Stream at wavelengths of $O(10)$ to $O(100)$ km [*Wang et al.*, 2010].

The Arctic Ocean is typically characterized as having low variability and weak levels of turbulence and mixing compared to other oceans [*Rainville et al.*, 2011]. This may be attributed to several factors, including that the presence of sea-ice and a strongly stratified upper ocean can act to damp atmospheric forcing [*Guthrie et al.*, 2013]. Additionally, much of the basin is north of the critical latitude of the semidiurnal M_2 tide (75°N), leading to relatively weak tidal forcing [*Kagan et al.*, 2010]. There have been very few studies of horizontal wavenumber spectra in the Arctic Ocean. *Timmermans et al.* [2012] examined horizontal variability under sea-ice within the Canada Basin during winter 2009/2010 using data from Ice Tethered Profilers (ITP). Horizontal wavenumber spectra of potential density (equivalent to potential energy) were found to scale like k^{-3} between 5 and 50 km wavelengths within the surface layer (10 m) and between scales of 10 and 50 km at depths of 60 m and 110 m. Equivalent scaling was also found between 0.5 and 20 km wavelengths within the surface layer of the shallow Chuckchi Sea under ice-free conditions [*Timmermans and Winsor*, 2013]. As highlighted by *Timmermans et al.* [2012] and *Timmermans and Winsor* [2013], the k^{-3} scaling of surface layer wavenumber spectra within these Arctic regions is steeper than that generally observed within regions of midlatitude open ocean and indicates less energy at small scales relatively to large scales.

The studies by *Timmermans et al.* [2012] and *Timmermans and Winsor* [2013] have primarily focussed on characterizing horizontal variability within the relatively fresh homogeneous surface layer of the Canadian Arctic. Below the surface layer is the halocline, a region generally extending to around 200 m where salinity and density increase rapidly and temperature decreases or remains close to freezing [*Morison et al.*, 1998; *Rudels*, 2001]. The halocline insulates the cold surface layer from a warmer Atlantic water layer which sits at 200–700 m depth. Without the halocline, surface waters would be exposed to the heat contained in the Atlantic water and there would be potential for increased sea-ice melt [*Steele and Boyd*, 1998]. The halocline layer, therefore, has a critical influence on ice melt and ice formation across the central Arctic Ocean which, in turn, has implications for freshwater content, thermohaline circulation, albedo, marine ecosystems, and ultimately Arctic governance and industry. We analyze a unique data set collected by a British submarine during summer 1996 in combination with historic CTD (conductivity-temperature-depth) and expendable CTD (XCTD) measurements to examine the dynamics of energy transfer at scales between 300 m and 50 km within the halocline of the Eurasian Arctic Ocean.

2. Data

British Royal Navy submarines have undertaken a number of data-gathering exercises within the Arctic Basin since 1971 [*Wadhams and Davis*, 2000; *Wadhams et al.*, 2011]. This study analyses underway data gained from an outboard CTD sensor during a voyage into the Arctic Basin in late summer 1996 (August–September). Calibrated temperature, salinity, and pressure data at a frequency of 1 Hz were obtained from the United Kingdom Hydrographic Office (UKHO).

For the derivation of horizontal wavenumber spectra, sections of temperature and salinity data were extracted along which the submarine traveled at approximately constant depth and speed. To be classified as approximately constant, variations in depth and speed were no more than ± 5 m and $\pm 25\%$

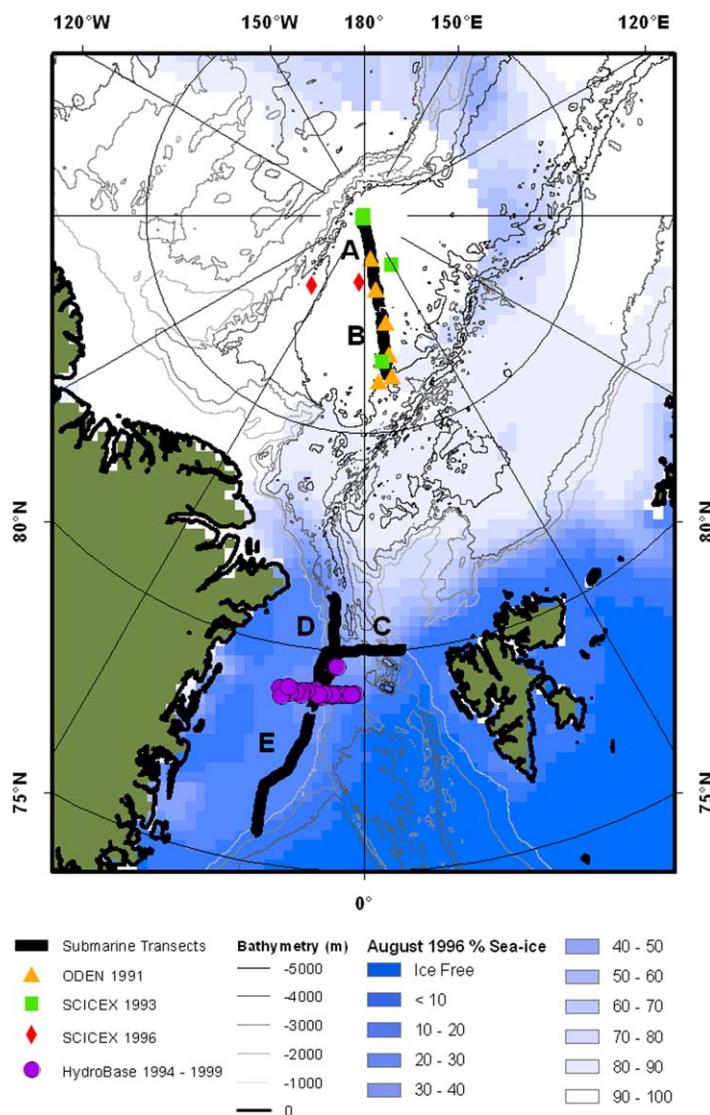


Figure 1. Positions of five sections of data where submarine depth and speed were approximately constant and the locations of depth profiles taken during summers (August–October) between 1991 and 1999. Summer sea-ice concentration (August 1996) and bathymetry contours are also shown.

profiles of temperature and salinity within the vicinity of the submarine transect were sought. Due to a lack of coincident data available for late summer 1996, data from summer months (August–October) in multiple years across the 1990s were used to produce climatological averages of water column structure. Within the Amundsen Basin, data collected as part of a cruise by the Swedish icebreaker Oden in 1991 [Anderson et al., 1994] along with data from the US SCICEX submarine programme in 1993 and 1996 were used (<http://www.ideo.columbia.edu/SCICEX/>) [Steele and Boyd, 1998]. Within Fram Strait and the East Greenland Shelf, 50 vertical profiles of temperature and salinity were downloaded from the HydroBase hydrographic database (<http://www.whoi.edu/hydrobase/php/index.php>) [Curry and Nobre, 2013].

3. Observations

Five transect sections were identified as having approximately constant depth and speed (Table 1). The maximum range in depth along each section was always <5 m and no correlation existed between depth variations and temperature or salinity. All sections were conducted within a short 10 day period overlapping the end of August and beginning of September. Of the five sections, two are within the Amundsen Basin under perennial sea-ice, two are within marginal sea-ice in Fram Strait and one is within marginal sea-ice on the East Greenland Shelf. Locations for each section are shown in Figure 1. Also shown are the locations of

(respectively) from the section average. Preliminary analysis indicated changes in these criteria do not significantly affect the position of recognizable peaks in the spectra or the spectral scaling.

Transects were categorized in terms of sea-ice cover using monthly 25 km resolution satellite sea-ice concentration data [Cavalieri et al., 1996, updated yearly]. Transects were taken to be under perennial ice if sea-ice concentrations were greater than 90% and within marginal ice when sea-ice concentrations were below 90% and greater than 15% (see Figure 1). It is assumed that sea-ice concentration was greater than 90% within the “pole hole” surrounding the North Pole where satellite data were absent. Data from the General Bathymetry Chart of the Ocean (GEBCO_08 Grid, version 20100927, <http://www.gebco.net>) which includes the International Bathymetric Chart of the Arctic Ocean (IBCAO) were used to examine the bathymetry of transects. Sea-ice concentration and bathymetric data were displayed and extracted for positions along each transect using ArcMap 10 GIS software.

To examine the stratification of the water column, vertical pro-

Table 1. Ice Cover, Bathymetry, Location and Transect Length Information for Five Sections of Data Where Depth and Velocity Were Approximately Constant

Transect ID	Length (km)	Average Depth (m) ± Standard Deviation	Location	Sea-Ice Cover Category	Average Bathymetry (m)
A	240	80 ± 0.3	Amundsen Basin	Perennial sea-ice	4246
B	175	80 ± 0.2	Amundsen Basin	Perennial sea-ice	4241
C	361	80 ± 0.2	Fram Strait	Marginal sea-ice	1161
D	290	80 ± 0.3	Fram Strait	Marginal sea-ice	2172
E	353	80 ± 0.3	East Greenland Shelf	Marginal sea-ice	357

vertical CTD and XCTD casts collected during summers between 1991 and 1999 within the vicinity of the submarine sections.

3.1. Vertical Water Column Structure

Within the Amundsen Basin, temperature and salinity data from vertical CTD and XCTD casts show a consistent water column structure (Figure 2a). A cold fresh surface layer, extending to 25–50 m, overlies the cold halocline where salinity increases rapidly and temperatures remain near freezing (this sharp transition is somewhat smoothed in the mean profile). Temperature begins to increase around 100 m depth and the warm Atlantic water layer is seen to be centered at approximately 300 m. The submarine sections within the Amundsen Basin (labeled A and B) are thus, at a depth of 80 m, located within the mid to lower part of the cold halocline layer [Aagaard *et al.*, 1981].

In central Fram Strait between 1°W and 4°W, temperature profiles are highly variable (Figure 2b). Several profiles indicate surface waters warmer than 0°C and temperature spikes as high as 5°C at 25–50 m. Salinity data indicate a fresh water surface layer approximately 10 m thick, below which sits the halocline. Profiles frequently indicate a step-like feature in the halocline at approximately 20–30 m, indicative of the effects of sea-ice melt [Steele and Boyd, 1998]. The presence of a cold halocline layer within this region appears variable and warm Atlantic water layer is centered at a depth of 200 m. The climatology suggests that, at a depth of 80 m, the sections within the Fram Strait (labeled C and D) are located within a halocline which has significant variation in temperature.

West of 4°W and over the East Greenland Shelf, surface temperatures are much less variable and consistent between profiles (Figure 2c). Data indicate a cold fresh surface layer extending to around 15–20 m ($S = 30$; $T = -0.5$) below which temperature decreases to near freezing down to approximately 100 m. Salinity increases below the surface layer with a strong halocline extending to approximately 200 m. Again profiles show evidence of summer ice melt indicated by the distinctive step in salinity at approximately 30 m visible in several profiles. The climatology indicates that the East Greenland Shelf section (labeled E) is within the climatological cold halocline layer.

3.2. Large Scale (>10 km) Horizontal Variability

No large scale horizontal features are seen in temperature or salinity along sections within the Amundsen Basin (Figures 3a and 3b). Sections A and B pass through a single water mass consistent with Lower Halocline Water (LHW) [Aksenov *et al.*, 2010; Morison *et al.*, 1998] centered on the 1027.5 kg m⁻³ density surface (Figures 4a and 4b). Bathymetry data indicate that section A overlies the flat abyssal plain with an average depth of 4246 m (Figure 3a). Section B mostly overlies similarly deep waters, however several sharp bathymetric features at depth associated with the Nansen-Grekkel Ridge are also present (Figure 3b).

Horizontal variations in temperature and salinity within the Fram Strait and the East Greenland Shelf indicate a number of structures greater than 10 km in size. Section C travels across a front, transitioning between warm saline waters into relatively cold fresh waters. Approximately 40 km from the frontal boundary, a mesoscale eddy-like structure with a diameter of $O(40)$ km consisting of similar warm water is clearly present (Figure 3c). It must be noted that there is no way of knowing whether the submarine passed through the center of any isolated coherent structure and therefore exact extent cannot be determined. The two distinct water masses present in section C are consistent with cold polar surface water (PSW; $\sigma < 27.7$; $T < 0$) and warm saline recirculated Atlantic water (RAW; $27.7 < \sigma < 27.9$; $T > 2$) [Rudels *et al.*, 2005]. Between these two water masses, transitional water is apparent between 1027.5 and 1028 kg m⁻³ isopycnals on either side of the mesoscale structure (Figure 4c). Section D similarly transits cold PSW and passes

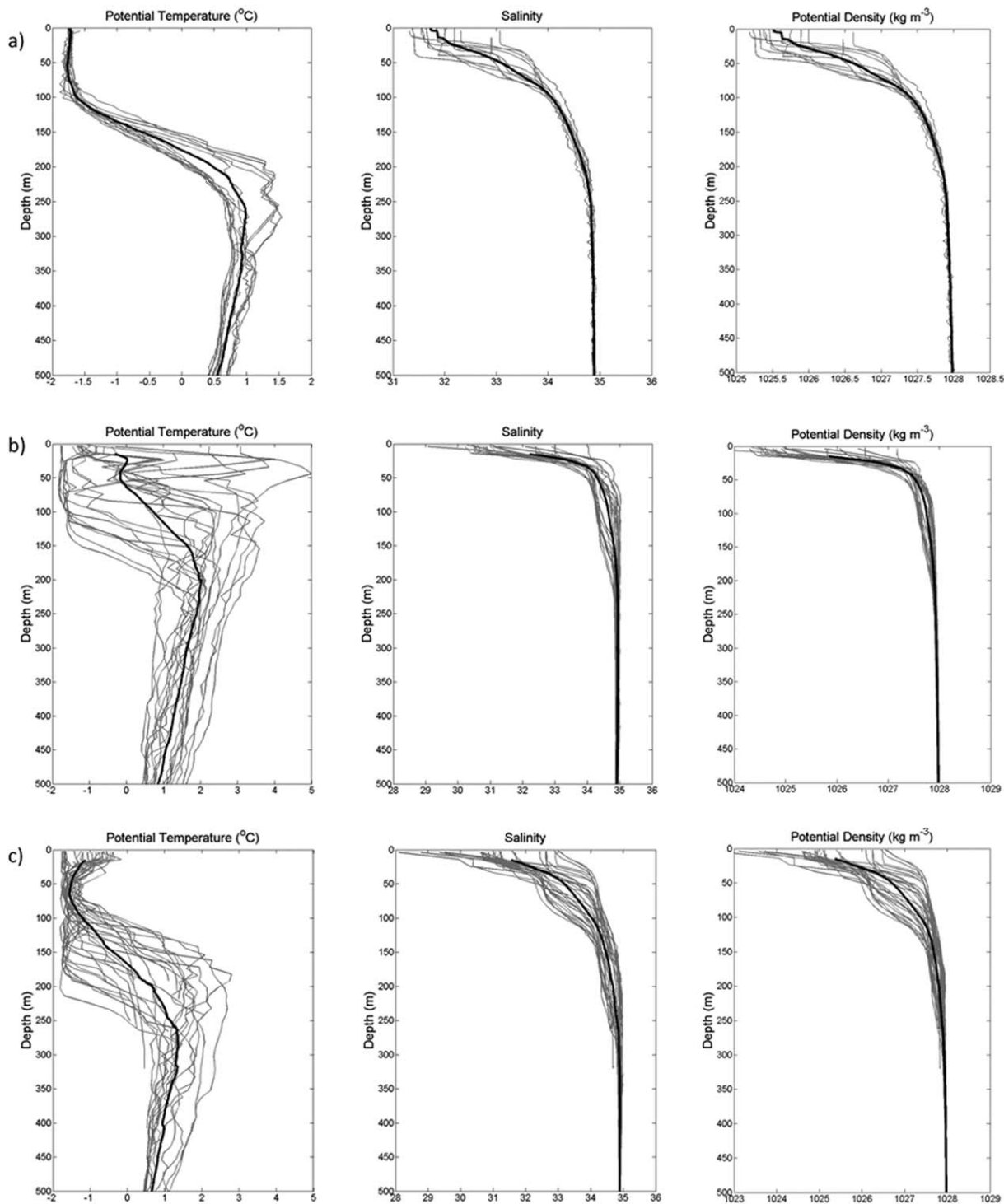


Figure 2. Climatology of summer vertical potential temperature (referenced to 0 dbar), salinity, and potential density (referenced to 0 dbar) structure within (a) the Amundsen Basin, (b) between 1°W and 4°W in Fram Strait, (c) west of 4°W in Fram Strait and on the Greenland shelf. Black solid line indicates calculated average, gray lines indicate individual profiles.

through a comparable warm saline mesoscale structure $O(30)$ km located along the continental slope (Figure 3d). Interestingly, the temperature of this structure is over 1°C less than that observed on section C, although it is still consistent with RAW, and the properties of the transitional water on either side of this feature differ considerably (Figure 4d).

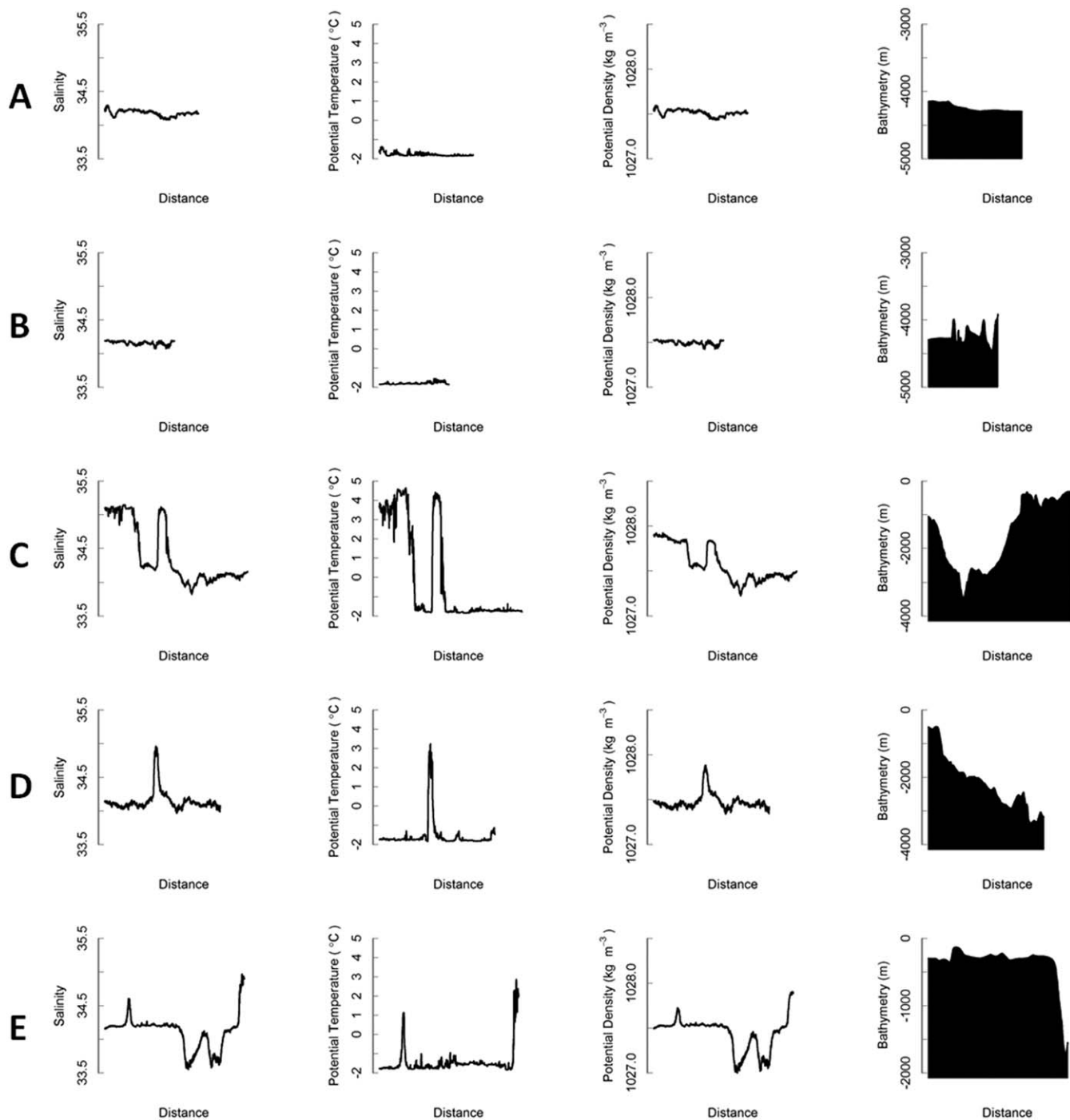


Figure 3. Horizontal variation in salinity, potential temperature, and potential density along transects A-E and estimated underlying bathymetry taken from GEBCO.

Horizontal variations in temperature and salinity along section E also indicate some interesting large scale horizontal variability. As with sections C and D, PSW dominates section E. However, evidence of Atlantic water is also present (Figure 4e). Increases in salinity and temperature are coincident with changes in bathymetry. A structure spanning $O(18)$ km is seen to be coincident with a sharp 200 m shoaling of the onshelf bathymetry while temperature also increases rapidly at the shelf break. Approaching the shelf break, salinity data indicate two structures $O(60)$ km associated with a significant decrease in salinity potentially indicating some form of active ice melt taking place or a freshwater plume (Figure 3e).

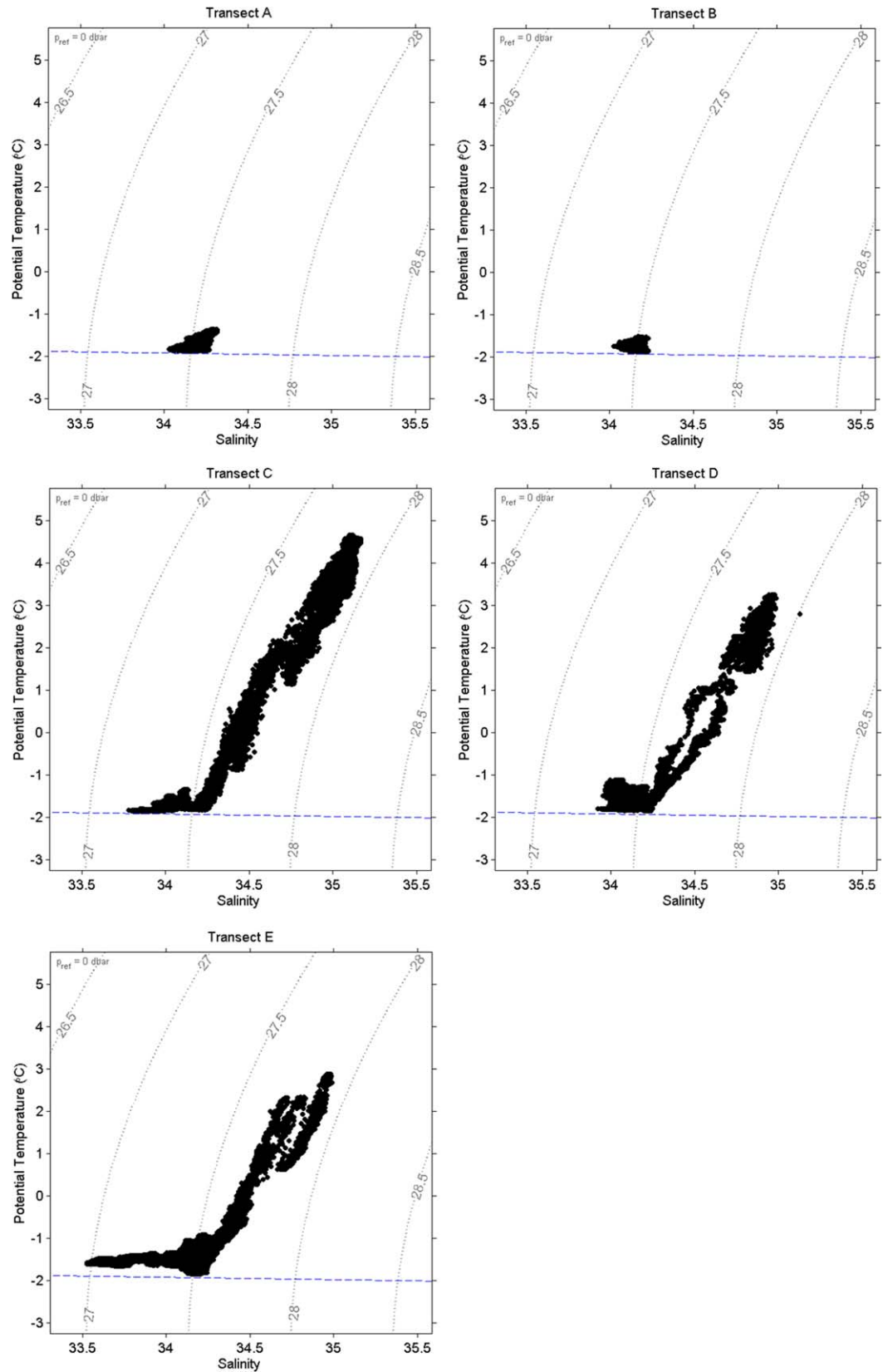


Figure 4. Potential temperature-salinity with σ contours for transects A-E. Dashed lines indicate freezing line at 0 dbar.

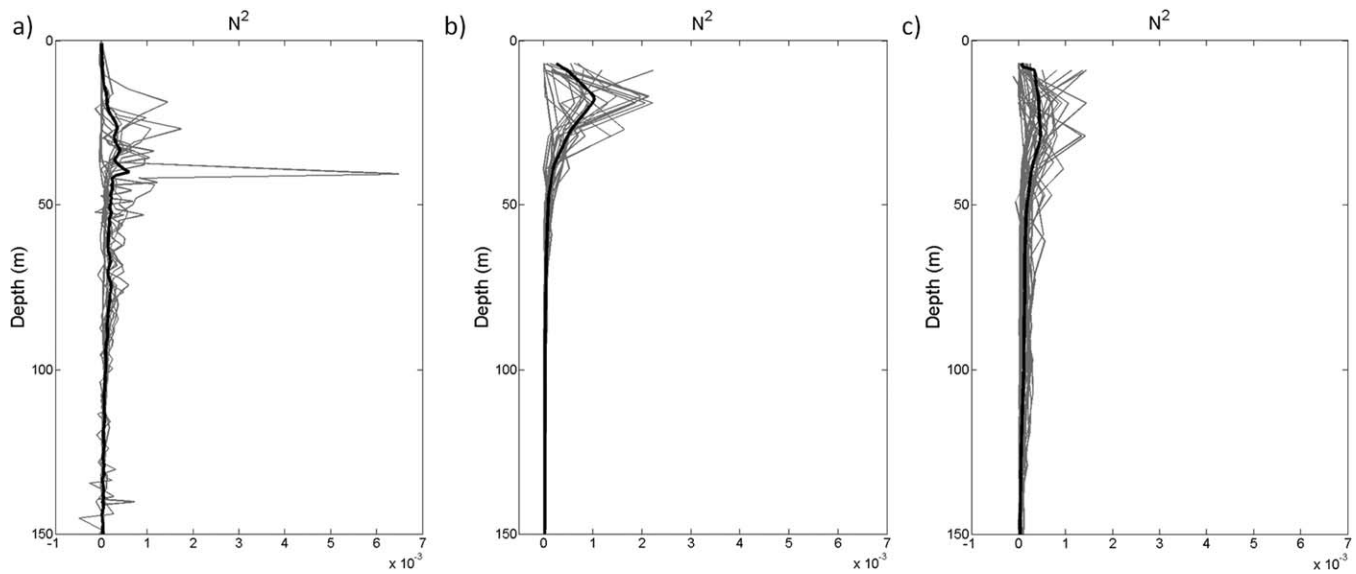


Figure 5. Climatology of Brunt-Väisälä frequency (N^2) within (a) the Amundsen Basin, (b) between 1°W and 4°W in Fram Strait, (c) west of 4°W in Fram Strait and on the East Greenland shelf.

4. Energy Spectra of Halocline Variability

4.1. Potential Energy

Potential energy can be expressed in terms of density using the hydrostatic balance and the local buoyancy frequency [Samelson and Paulson, 1988],

$$\text{Potential Energy} = (g/N)^2 [(\rho - \rho_0)/\rho_0]^2 \quad (1)$$

where g is the local gravitational acceleration, N is the Brunt-Väisälä frequency, ρ is density, and ρ_0 is a constant reference density (here 1000 kg m^{-3}).

Potential energy along each of the five submarine sections (A-E) was calculated following equation (1). Horizontal density variations were calculated from observations of temperature and salinity following protocols in the SeaWater oceanographic toolbox based on Fofonoff and Millard [1983] and Millero *et al.* [1980]. Estimates of the local Brunt-Väisälä frequency (N) at the vessel depth were gained from vertical CTD and XCTD climatology following equation (3.7.15) in Gill [1982] (Figure 5). Frequencies were estimated to be $1.2 \times 10^{-2} (\pm 1.2 \times 10^{-3}) \text{ s}^{-1}$, $5.5 \times 10^{-3} (\pm 3.2 \times 10^{-4}) \text{ s}^{-1}$, and $1.0 \times 10^{-2} (\pm 7.4 \times 10^{-4}) \text{ s}^{-1}$ in the Amundsen Basin, Fram Strait, and East Greenland Shelf, respectively. Profiles of N^2 reveal the water column is more stable within the Amundsen Basin and on the East Greenland Shelf than within Fram Strait. At the depth of interest, 80 m, values for N calculated from profiles in different years were in good agreement (Figure 5).

4.2. Calculating Spectra

Potential energy spectra are calculated and analyzed for sections A-E. The common fast-tow approximation is made when calculating wavenumber spectra, which assumes that the turbulence field is effectively frozen because the vessel traverses each of the scales of interest at a speed much greater than naturally occurring perturbations [Thorpe, 2007]. This approximation is appropriate as submarine speeds are $>3 \text{ m s}^{-1}$, and hence are at least 10 times greater than the maximum water current speeds (~ 0.01 and 0.15 m s^{-1} in the central Arctic basin and East Greenland Current, respectively) and at least five times the typical eddy propagation speeds ($O(10) \text{ cm s}^{-1}$) [Aagaard *et al.*, 2008; Aagaard and Coachman, 1968]. Data along each section are averaged to 15 s bins to reduce high frequency noise and aliasing. Horizontal resolution corresponding to the 15 s average is in the range of 45–75 m. The mean was removed from each section time series and a cosine bell taper applied to 10% of the data at each end to reduce side-lobe leakage and end effects. Spectra were calculated for each section following equation (2) [Emery and Thomson, 2001]

$$PSD(f) = \frac{2}{n\Delta t} |Y(f)|^2 \quad (2)$$

where PSD is the one-sided power spectral density at frequency f , $Y(f)$ is the Fourier component of a series with n data points at discrete frequencies $f = j/[n\Delta t]$, $j = 0, 1, \dots, [n/2] - 1$ obtained through Fast Fourier Transform (FFT) and Δt is the sampling interval. Spectra are smoothed using a modified Daniell window with width 7 equivalent to a bandwidth of $B_w = 0.48$ [Cowperrwait and Metcalfe, 2009; Percival and Walden, 1993]. We convert frequency ($\sigma = 2\pi/t$) spectra, derived from the time series collected along each section at a speed U , to wavenumber ($k = \sigma/U$) spectra in terms of distance (x), where $x = Ut$ and $k = 2\pi/x$. This method of determining wavenumber spectra from a time series using submarine speed provided results that are indistinguishable from those gained through interpolation of distance. The presence of the front in section C was of some concern as it could potentially bias the gradient of the resulting spectrum toward a k^{-2} slope [Franks, 2005]. However, analysis indicated that removing the frontal feature from section C made no statistically significant difference to the results presented in the following section (data not shown).

4.3. Potential Energy Spectra

Potential energy spectra between wavelengths of 300 m and 50 km for submarine sections within the Amundsen Basin, Fram Strait, and East Greenland Current are shown in Figure 6. Results indicate that horizontal variability in the marginal sea-ice of Fram Strait is an order of magnitude more energetic than that in the East Greenland Shelf MIZ and two orders of magnitude more energetic than under the perennial sea-ice of the Amundsen Basin. However, the shapes of the potential energy spectra are similar within the three Arctic regions despite differences in sea-ice cover. In general spectra fall off steeply from 50 km down to a transition wavelength (L_T) and then flatten out at smaller scales down to 300 m. This transition wavelength occurs at scales between approximately 5 and 7 km with L_T for sections in the Amundsen Basin occurring at larger wavelengths (smaller wavenumbers) than those within Fram Strait and East Greenland Shelf (Figures 6a–6e and Table 2). At wavelengths between L_T (5–7 km) and 50 km, spectral slopes for all sections are steeper (sections D and E) or statistically indistinguishable (sections A, B, and C) from a k^{-3} scaling (Table 2).

Charney [1971] predicted that for three-dimensional quasigeostrophic turbulence, away from surface boundaries, energy spectra at wavenumbers greater than the baroclinic production range scale like k^{-3} . The theory assumes that energy is extracted from the mean flow through baroclinic instability at scales close to the deformation radius and dissipation is negligible so nonlinear interactions lead to a forward cascade of enstrophy from large to small scales. The spectral slope predicted by Charney [1971] for three-dimensional quasigeostrophic turbulence across the enstrophy range can be directly mapped to two dimensional quasigeostrophic flow. For energy spectra derived from one-dimensional (along track) observations, the k^{-3} power law dependency is unchanged. The first baroclinic deformation radius (R_1) is approximately 8 km in the Amundsen Basin and 5 km in Fram Strait and Greenland Sea [Nurser and Bacon, 2014]. This is equivalent to a first deformation wavelength (L_1) between 50 and 30 km, where $L_1 = 2\pi R_1$. The scale for the fastest growing wavelength of quasigeostrophic instability (or dominant mode) is typically near or some multiple of the deformation wavelength [Allen et al., 1994; Tulloch et al., 2011]. Therefore, spectra between L_T and 50 km length scales within the different Arctic regions are consistent with interior quasigeostrophic (QG) turbulence theory suggesting stirring related to baroclinic instability.

At scales below L_T down to 300 m, the slope of the energy spectral scaling becomes significantly less steep and appear close to a $k^{-5/3}$ scaling or flatter (Figure 6), although there is variability between sections (Table 2). It should be noted that the relatively large number of data points at this end of the spectra, compared to those at larger scales, lead to smaller confidence intervals on the calculated gradients and that these do not account for uncertainties associated with other potential sources of noise such as that from vessel movement or instrument noise. Nevertheless, these slopes are much flatter than those at larger wavelengths and are not consistent with interior QG dynamics and stirring from baroclinic instability, suggesting different dynamics dominate at small scales between 300 m and L_T (~5–7 km).

5. Discussion

Determining how energy is transferred across spatial scales is a fundamental question of ocean dynamics. Within the upper ocean, horizontal density variations formed by eddies, fronts, and ageostrophic motions are thought

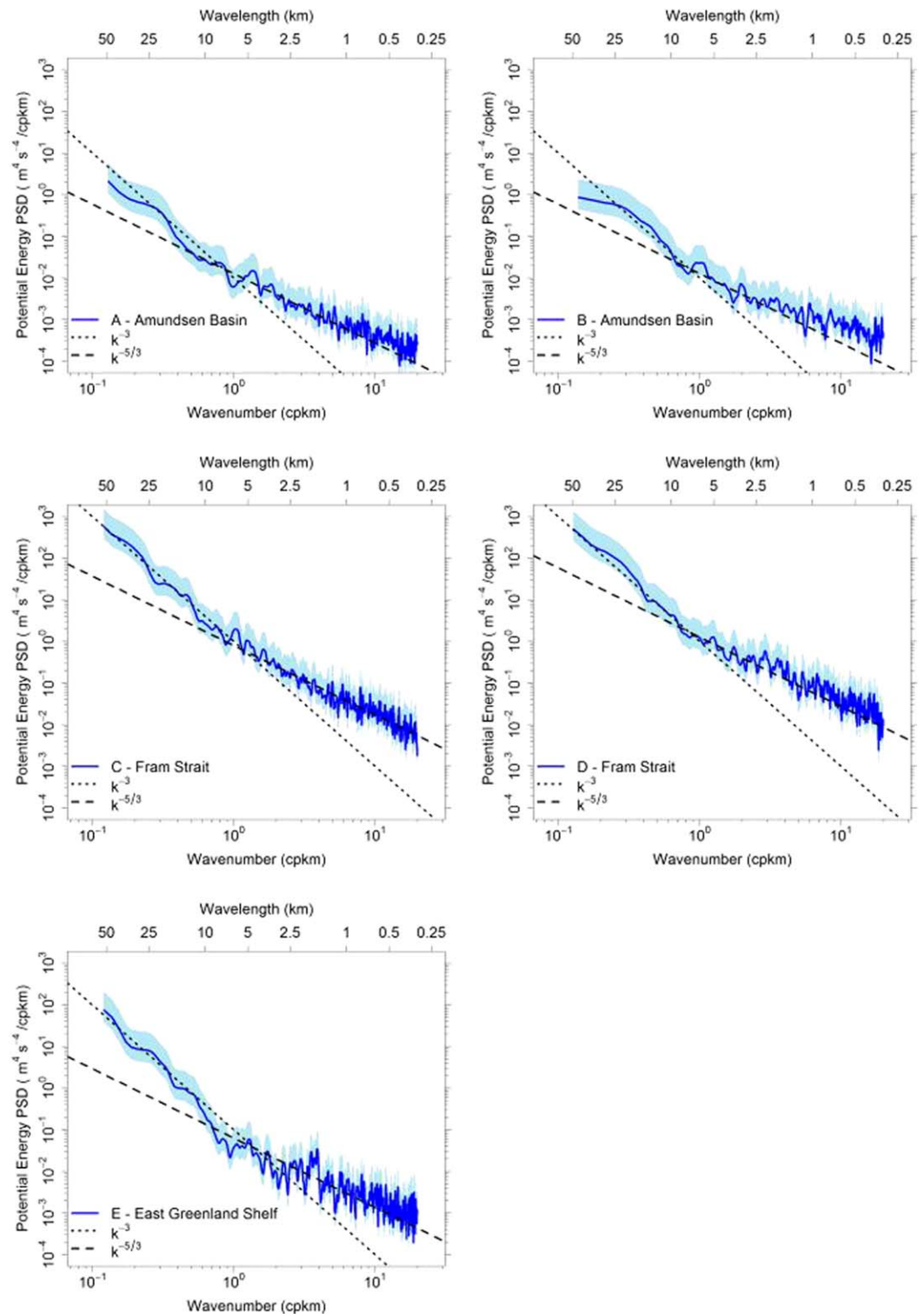


Figure 6. Potential energy spectra for length scales between 300 m and 50 km within Amundsen Basin, Fram Strait and on the East Greenland Shelf in the Eurasian Arctic. Shaded areas indicate 95% confidence intervals.

to play an important dynamical role up to scales at least $O(100)$ km and influence the cascade of energy and enstrophy to dissipation scales [Capet *et al.*, 2008a]. However, there is still much uncertainty surrounding the processes governing how energy is transferred across scales. Furthermore, very few studies have examined horizontal variability in the upper Arctic Ocean where horizontal density gradients in the upper layers of the water

Table 2. Calculated Spectral Slopes and Integrated Spectral Density for Horizontal Variations of Potential Energy Between Given Wavelengths

Section	Wavelength (km; $L = 2\pi/k$)	Spectral Slope	Integrated PSD
A	50–6.3	-2.81 ± 0.26	0.0017
B	50–7.3	-2.64 ± 0.54	0.0017
C	50–5.4	-2.92 ± 0.21	0.3580
D	50–6.1	-3.19 ± 0.16	0.3609
E	50–5.1	-3.54 ± 0.22	0.0349
A	6.3–0.3	-1.30 ± 0.05	0.0002
B	7.3–0.3	-1.09 ± 0.06	0.0003
C	5.4–0.3	-1.62 ± 0.04	0.0103
D	6.1–0.3	-1.51 ± 0.06	0.0201
E	5.1–0.3	-1.24 ± 0.07	0.0008

column occur, not only via cascading of existing gradients through horizontal stirring, but also from processes such as ice formation and brine rejection [Timmermans *et al.*, 2012]. This study has examined horizontal variability and associated potential energy spectra using rare high frequency data collected by a Royal Navy submarine from Arctic regions with differing sea-ice conditions. These data, combined with estimates of Brunt-Väisälä frequency, calculated from historic CTD and XCTD measurement, have allowed the calculation of potential energy spectra for the halocline layer within the Eurasian Arctic Ocean at length scales between 300 m and 50 km.

5.1. Energy Distribution Across the Mesoscale (L_T –50 km)

Results from this study indicate that, between 50 km and a transition wavelength L_T (ranging between ~ 5 and 7 km), horizontal potential energy spectra within the Amundsen Basin perennial sea-ice and the Fram Strait and the East Greenland shelf MIZ scale like k^{-3} . This is consistent with interior QG turbulence theory and stirring related to baroclinic instabilities. The results presented in Figure 6 indicate no distinguishable differences in the scaling of energy spectra across a variety of sea-ice concentrations during summer in the Eurasian Basin at wavelengths between L_T and 50 km. However, the magnitude of potential energy variance does differ considerably between Arctic regions. This indicates differences in the strength of the sources driving the observed variability, which is likely to be linked not only to ice-cover but also to the differences in geographical location and proximity to energetic boundary currents. For example, vertical shear between the East Greenland Current and recirculated Atlantic water and wind driven ice edge jets are sources of high mesoscale variability in Fram Strait [Johannessen *et al.*, 1987]. In contrast, low mesoscale variability in the central Eastern Arctic has previously been attributed to rapid decay of eddies from the MIZ as they enter the perennial ice-covered regions of the central basin [Muench, 1990].

The k^{-3} scaling of potential energy spectra observed between L_T and 50 km is in agreement with findings within the surface layer under sea-ice in Canada Basin during winter [Timmermans *et al.*, 2012] and the surface layer of the ice-free Chuckchi Sea during summer [Timmermans and Winsor, 2013]. This scaling is steeper than the k^{-2} scaling more commonly observed within the mixed layer and thermocline of midlatitude open oceans [Cole *et al.*, 2010; Ferrari and Rudnick, 2000; Katz, 1975] and model simulations [Capet *et al.*, 2008b; Klein *et al.*, 2008]. Timmermans *et al.* [2012] suggest that the steeper k^{-3} scaling indicates that dynamical processes and instability within the Arctic Ocean are potentially being altered by the presence of sea-ice. The fact that spectral scaling does not vary with sea-ice concentration would suggest that dynamics are altered by seasonal sea-ice presence not only permanent sea-ice cover. It must be noted however that, although less common, observations of k^{-3} scaling of horizontal potential energy spectra exist within the mixed layer for open oceans outside of the Arctic [Samelson and Paulson, 1988; Wang *et al.*, 2010] and the mechanisms driving the differences in spectra scaling are not fully understood. The similarities in scaling of spectra from different Arctic regions suggest dynamics are not directly related to sea-ice concentration. Instead, the influence of sea-ice on stratification may be more important in affecting energy transfer across horizontal scales. Indeed, a number of recent model and observational studies have suggested that the stratification, rather than the amount of open water, is a key factor in determining the energy and mixing potential of turbulent processes within the Arctic Ocean [Gimbert *et al.*, 2012a, 2012b; Guthrie *et al.*, 2013].

5.2. Energy Distribution at Small Scales ($<L_T$)

The high frequency nature of the environmental data used in this study allows spectra to be examined down to length scales $O(100)$ m. As k increases a pronounced transition in spectral scaling from k^{-3} to $k^{-5/3}$ or flatter is observed to occur at a wavenumber between 8.6×10^{-1} and 1.24 cpkm, depending on the submarine section. Such a flattening in spectra could potentially be attributed to noise contamination. There is potential for noise in the data due to high frequency perturbations created by the submarine moving through the water. However, numerical studies show that the drag disturbances around the hull of a long thin propelled body in a high Reynolds number have a length scale less than the length of the hull [Karim *et al.*, 2009]. Thus,

the 300 m lower bound set on spectra is substantially larger than the scales at which any noise due to vessel movement would occur. Furthermore, the averaging of data into 15 s bins, prior to the calculation of spectra, acted as low-pass filter to smooth any noise at high wavenumbers (equivalent to horizontal lengths between 45 and 75 m) present due to either instrumental noise or vessel movement. The observed transition in the spectrum to a flatter scaling is therefore thought to be a real feature and not an artifact of noise in the data.

The spectra found in this study for regions of the Arctic Ocean are extremely similar in nature to those found for the troposphere in the atmosphere, which show a transition from a k^{-3} scaling at synoptic scales to a $k^{-5/3}$ scaling at smaller scales [Nastrom and Gage, 1985]. There have been multiple explanations suggested for the transition in scaling observed in troposphere potential energy and kinetic energy spectra, however, full theoretical understanding remains elusive. Several studies have suggested that a $k^{-5/3}$ scaling within atmospheric horizontal wavenumber spectra at small wavelengths is indicative of internal-gravity waves [Dewan, 1979; Van Zandt, 1982] or inertia-gravity waves (internal waves affected by rotation) [Callies et al., 2014]. Gage and Nastrom [1986] suggested that the regime of $k^{-5/3}$ scaling signifies an inverse energy cascade from small to larger scales with energy input from the breaking of propagating internal waves as the small scale source, and a sink at the scale at which the spectrum flattens. However, it must be noted that numerical studies have found little evidence to support such an inverse cascade [Cho and Lindborg, 2001].

Within the ocean, Callies and Ferrari [2013] reanalyzed the Atlantic Gulf Stream data originally studied by Wang et al. [2010] and found a flattening of energy spectra from k^{-3} to k^{-2} at scales <20 km within the mixed layer and the thermocline. This flattening was consistent with predicted Garrett and Munk (GM) spectrum [Garrett and Munk, 1975] and was thought to indicate internal wave dynamics dominating energy at small wavelengths. A similar pattern can be seen in energy spectra from the upper pycnocline derived from data collected during the LatMix experiment in the North Atlantic Mode Water region [Scherbina et al., 2013, Figure 4c] indicate that observed and model spectra are in agreement at scales >20 km but diverge at smaller scales with the discrepancy attributed to the lack of representation of internal waves within the model. This was supported by observed spectra at wavelengths below 20 km close to GM predictions. Furthermore, Bühler et al. [2014] decomposed the horizontal velocity Gulf Stream data set from Wang et al. [2010] into its wave and balanced components and found that the inertia-gravity wave component dominates at scales <20 km.

Within this study, the slopes of horizontal potential energy spectra at scales between the L_T to 300 m are shallower than predicted by the GM model. However, the GM model is based primarily on observations from mid-latitudes. Previous studies have found internal wave energy to be one to two orders of magnitude less under Arctic sea-ice than in other oceans and the wave spectrum to be flatter than predicted by the GM model [D'Asaro and Morison, 1992; Levine et al., 1987; Pinkel, 2005]. Therefore the flattening of potential energy spectra observed at scales of ~ 5 –7 km within the Arctic Ocean halocline may still be consistent with internal wave variability. The impact of sea-ice may explain the differences observed because it can significantly influence generation and dissipation mechanisms of the wave field. Sea-ice limits wind stress transfer from the atmosphere to the upper ocean reducing inertial forcing while ice keels can generate high frequency internal waves as ice moves relative to the ocean surface layer. Sea-ice may also increase dissipation rates through increased friction at the ice/ocean boundary compared to air/ocean boundary in ice-free oceans [Padman, 1995].

The transition observed in tropospheric spectra has also been suggested to represent the superposition of an interior QG dominated forward enstrophy cascade at large scales and a forward cascade of surface energy consistent with surface quasigeostrophic theory (SQG) at small scales [Tulloch and Smith, 2009]. SQG theory, as described by Blumen [1978], predicts a $k^{-5/3}$ scaling of energy spectra and serves as a counterpart to interior QG theory, accounting for buoyancy anomalies near the surface while assuming uniform interior potential vorticity [Klein et al., 2008]. SQG dynamics have been shown to be relevant to the upper ocean in the first 500 m [Capet et al., 2008a] with correlations found between potential vorticity anomalies driving mesoscales and density/buoyancy anomalies driving small scale surface frontogenesis [Klein et al., 2008, 2011; Lapeyre and Klein, 2006]. The typical k^{-2} scaling of energy spectra from open oceans at midlatitudes is said to be consistent with SQG dynamics accounting for ageostrophic motions [Klein et al., 2008]. The flattening of potential energy spectra observed within the Arctic halocline could be consistent with a transition from interior QG dominated dynamics to SQG dominated dynamics at small scales. However, all variants of SQG theory include a decay of the surface mode with distance into the interior, with smaller scales decaying at a faster rate. For the case presented here the identity of the "surface" is not clear (water surface and top and bottom of pycnocline are all possibilities) so, even putting aside issues related to the strongly nonuniform stratification, it is uncertain how modified, through such decay with depth, any theoretical

prediction from an SQG theory may be at the depth studied. It is also noted that below the transition wavelength spectral scaling is statistically flatter than k^{-2} in all sections and flatter than $k^{-5/3}$ in all but section C (Table 2).

It may not be possible to relate the flattening of spectra observed at small scales to one current theoretical theorem. However, from a dynamical perspective, it is interesting to note that there is considerable variation in scaling between transects at wavelengths from L_T to 300 m. These variations may indicate differences in the mechanisms driving small scale ($<L_T$) dynamics at different locations (e.g., bathymetry, air-ice-ocean stress, ice melt, ice formation, etc.). For example, spectra generally appear flatter in the perennial sea-ice than in the MIZ which may be indicative of high frequency internal waves generated by ice keels as sea-ice moves relative to the underlying ocean. Further data are required to examine the spatial and temporal extent of this small scale variability and investigate its cause.

6. Conclusion

Little is known regarding the transfer of energy by turbulent processes across the mesoscale to smaller scales especially within the presence of sea-ice. Horizontal potential energy spectra indicate potential differences in the pathways for energy exchange within the Arctic Ocean compared to open ocean regions. Within the Arctic halocline, energy spectra are consistent with interior QG dynamics dominating scales between ~ 5 – 7 and 50 km. This scaling is steeper than typically found in regions of midlatitude open ocean and implies relatively less energy at scales representative of submesoscale dynamics and ageostrophic motions. Similarities in the scaling of spectra across regions of differing sea-ice concentration suggest that upper ocean stratification, rather than the amount of open water, may play a role in altering the dynamics of energy transfer. At wavelengths between 300 m and ~ 5 – 7 km, spectral scaling is flatter indicating a change in dynamics, potentially due to internal waves dominating variability. Spectral analysis also indicates significant variability in potential energy variance across differing Arctic regions indicating differences in the strength of sources responsible for the observed variability. Understanding the energy exchange pathways within the presence of sea-ice and how these may change in future is important for Arctic modeling efforts, particularly for parameterization of turbulent processes at scales finer than models can resolve.

Acknowledgments

This research was supported by the SEATS project (grant NE/1028408/1) funded by the UK Natural Environment Research Council as part of their Arctic Research Programme. We acknowledge the United Kingdom Hydrographic Office (UKHO) and Defence Science Technology Laboratory (DSTL) for providing access to data collected from the Royal Navy submarine (data are held by UKHO, access is restricted). We specifically thank Steve Lock and Garry Dawson for their help and assistance. We also thank Patrice Klein, Xavier Capet, and Shafer Smith for a number of extremely useful discussions. We acknowledge the Forum for Arctic Modeling and Observational Synthesis (FAMOS) and Wendy Ermold for help obtaining the Oden and SCICEX profile data (sourced from WERMOLD@apl.washington.edu), the British Oceanographic Data Centre for maintaining the GEBCO bathymetric chart (sourced from <http://www.bodc.ac.uk/projects/international/gebco/>), and Woods Hole Oceanographic Institution for maintaining HydroBase (data sourced from http://www.whoi.edu/science/PO/hydrobase/php/data_download.php). We also thank the two anonymous reviewers for their helpful suggestions and advice in improving the paper.

References

- Aagaard, K., and L. K. Coachman (1968), The East Greenland Current North of Denmark Strait: Part I, *Arctic*, 21(3), 181–200.
- Aagaard, K., L. K. Coachman, and E. Carmack (1981), On the halocline of the Arctic Ocean, *Deep Sea Res., Part A*, 28(6), 529–545, doi:10.1016/0198-0149(81)90115-1.
- Aagaard, K., R. Andersen, J. Swift, and J. Johnson (2008), A large eddy in the central Arctic Ocean, *Geophys. Res. Lett.*, 35, L09601, doi:10.1029/2008GL033461.
- Aksenov, Y., S. Bacon, A. C. Coward, and N. P. Holliday (2010), Polar outflow from the Arctic Ocean: A high resolution model study, *J. Mar. Syst.*, 83(1–2), 14–37, doi:10.1016/j.jmarsys.2010.06.007.
- Allen, J. T., D. A. Smeed, and A. L. Chadwick (1994), Eddies and mixing at the Iceland-Færøe front, *Deep Sea Res., Part I*, 41(1), 51–79, doi:10.1016/0967-0637(94)90026-4.
- Anderson, L. G., G. Björk, O. Holby, E. P. Jones, G. Kattner, K. P. Koltermann, B. Liljeblad, R. Lindegren, B. Rudels, and J. Swift (1994), Water masses and circulation in the Eurasian Basin: Results from the Oden 91 expedition, *J. Geophys. Res.*, 99(C2), 3273–3283, doi:10.1029/93JC02977.
- Blumen, W. (1978), Uniform potential vorticity flow: Part I. Theory of wave interactions and two-dimensional turbulence, *J. Atmos. Sci.*, 35, 774–783.
- Bühler, O., J. Callies, and R. Ferrari (2014), Wave-vortex decomposition of one-dimensional ship-track data, *J. Fluid Mech.*, 756, 1007–1026.
- Callies, J., and R. Ferrari (2013), Interpreting energy and tracer spectra of upper-ocean turbulence in the submesoscale range (1–200 km), *J. Phys. Oceanogr.*, 43(11), 2456–2474, doi:10.1175/JPO-D-13-063.1.
- Callies, J., R. Ferrari, and O. Bühler (2014), Transition from geostrophic turbulence to inertia-gravity waves in the atmospheric energy spectrum, *Proc. Natl. Acad. Sci. U. S. A.*, 111(48), 17,033–17,038, doi:10.1073/pnas.1410772111.
- Capet, X., P. Klein, B. L. Hua, G. Lapeyre, and J. C. McWilliams (2008a), Surface kinetic energy transfer in surface quasi-geostrophic flows, *J. Fluid Mech.*, 604, 165–174, doi:10.1017/S0022112008001110.
- Capet, X., J. C. McWilliams, M. J. Molemaker, and A. F. Shchepetkin (2008b), Mesoscale to submesoscale transition in the California Current System. Part I: Flow structure, eddy flux, and observational tests, *J. Phys. Oceanogr.*, 38(1), 29–43, doi:10.1175/2007JPO3671.1.
- Cavaliere, D. J., C. L. Parkinson, P. Gloersen, and H. J. Zwally (1996, updated yearly), *Sea Ice Concentrations From Nimbus-7 SMMR and DMSP SSM/I-SSMIS Passive Microwave Data: August 1996–September 1996*, Natl. Snow and Ice Data Cent., Boulder, Colo.
- Charney, J. G. (1971), Geostrophic turbulence, *J. Atmos. Sci.*, 28(6), 1087–1095, doi:10.1175/1520-0469(1971)028<1087:GT>2.0.CO;2.
- Cho, J. Y. N., and E. Lindborg (2001), Horizontal velocity structure functions in the upper troposphere and lower stratosphere: 1. Observations, *J. Geophys. Res.*, 106(D10), 10,223–10,232, doi:10.1029/2000JD900814.
- Cole, S. T., D. L. Rudnick, and J. A. Colosi (2010), Seasonal evolution of upper-ocean horizontal structure and the remnant mixed layer, *J. Geophys. Res.*, 115, C04012, doi:10.1029/2009JC005654.
- Comiso, J. C., C. L. Parkinson, R. Gersten, and L. Stock (2008), Accelerated decline in the Arctic sea ice cover, *Geophys. Res. Lett.*, 35, L01703, doi:10.1029/2007GL031972.
- Cowpervait, P. S. P., and A. V. Metcalfe (2009), *Introductory Time Series With R*, Springer, London, U. K., doi:10.1007/978-0-387-88698-5.
- Curry, R., and C. Nobre (2013), *Hydrobase3*, technical report, 38 pp., Woods Hole Oceanogr. Inst. [Available at http://www.whoi.edu/hydrobase/docs/TechReport_03Sep2013.pdf].

- D'Asaro, E. A., and J. H. Morison (1992), Internal waves and mixing in the Arctic Ocean, *Deep Sea Res., Part A*, 39(2), S459–S484, doi:10.1016/S0198-0149(06)80016-6.
- Dewan, E. M. (1979), Stratospheric wave spectra resembling turbulence, *Science*, 204(4395), 832–835, doi:10.1126/science.204.4395.832.
- Emery, W. J., and R. E. Thomson (2001), Time-series analysis methods, in *Data Analysis Methods in Physical Oceanography*, edited by W. J. Emery and R. E. Thomson, pp. 371–567, Elsevier Sci., Amsterdam, doi:10.1016/B978-044450756-3/50006-X.
- Ferrari, R., and D. L. Rudnick (2000), Thermohaline variability in the upper ocean, *J. Geophys. Res.*, 105(C7), 16,857–16,883, doi:10.1029/2000JC900057.
- Fofonoff, N. P., and R. C. Millard (1983), *Algorithms for Computation of Fundamental Properties of Seawater*, United Nations Educational, Scientific and Cultural Organization (UNESCO), Paris.
- Franks, P. J. S. (2005), Plankton patchiness, turbulent transport and spatial spectra, *Mar. Ecol. Prog. Ser.*, 294, 295–309, doi:10.3354/meps294295.
- Gage, K. S., and G. D. Nastrom (1986), Theoretical interpretation of atmospheric wavenumber spectra of wind and temperature observed by commercial aircraft during GASP, *J. Atmos. Sci.*, 43(7), 729–740, doi:10.1175/1520-0469(1986)043<0729:TIOAWS>2.0.CO;2.
- Garrett, C., and W. Munk (1975), Space-time scales of internal waves: A progress report, *J. Geophys. Res.*, 80(3), 291–297, doi:10.1029/JC080i003p00291.
- Gill, A. E. (1982), *Atmosphere-Ocean Dynamics*, Academic, San Diego, Calif.
- Gimbert, F., N. C. Jourdain, D. Marsan, J. Weiss, and B. Barnier (2012a), Recent mechanical weakening of the Arctic sea ice cover as revealed from larger inertial oscillations, *J. Geophys. Res.*, 117, C00J12, doi:10.1029/2011JC007633.
- Gimbert, F., D. Marsan, J. Weiss, N. C. Jourdain, and B. Barnier (2012b), Sea ice inertial oscillations in the Arctic Basin, *Cryosphere*, 6(5), 1187–1201, doi:10.5194/tc-6-1187-2012.
- Guthrie, J. D., J. H. Morison, and I. Fer (2013), Revisiting internal waves and mixing in the Arctic Ocean, *J. Geophys. Res. Oceans*, 118, 3966–3977, doi:10.1002/jgrc.20294.
- Johannessen, J. A., et al. (1987), Mesoscale eddies in the Fram Strait marginal ice zone during the 1983 and 1984 Marginal Ice Zone Experiments, *J. Geophys. Res.*, 92(C7), 6754–6772, doi:10.1029/JC092iC07p06754.
- Kagan, B. A., A. A. Timofeev, and E. V. Sofina (2010), Seasonal variability of surface and internal M2 tides in the Arctic Ocean, *Izv. Russ. Acad. Sci. Atmos. Oceanic Phys.*, 46(5), 652–662, doi:10.1134/S0001433810050105.
- Karim, M. M., M. M. Rahman, and M. A. Alim (2009), Computation of turbulent viscous flow around submarine hull using unstructured grid, *J. Ship Technol.*, 5(1), 973–1423.
- Katz, E. J. (1975), Tow spectra from MODE, *J. Geophys. Res.*, 80(9), 1163–1167, doi:10.1029/JC080i009p01163.
- Klein, P., B. L. Hua, G. Lapeyre, X. Capet, S. Le Gentil, and H. Sasaki (2008), Upper ocean turbulence from high-resolution 3D simulations, *J. Phys. Oceanogr.*, 38(8), 1748–1763, doi:10.1175/2007jpo3773.1.
- Klein, P., G. Lapeyre, G. Roullet, S. L. Gentil, and H. Sasaki (2011), Ocean turbulence at meso and submesoscales: Connection between surface and interior dynamics, *Geophys. Astrophys. Fluid Dyn.*, 105, 421–437, doi:10.1080/03091929.2010.532498.
- Kwok, R., G. F. Cunningham, M. Wensnahan, I. Rigor, H. J. Zwally, and D. Yi (2009), Thinning and volume loss of the Arctic Ocean sea ice cover: 2003–2008, *J. Geophys. Res.*, 114, C07005, doi:10.1029/2009JC005312.
- Lapeyre, G., and P. Klein (2006), Dynamics of the upper oceanic layers in terms of surface quasigeostrophy theory, *J. Phys. Oceanogr.*, 36(2), 165–176, doi:10.1175/JPO2840.1.
- Levine, M. D., C. A. Paulson, and J. H. Morison (1987), Observations of internal gravity waves under the Arctic pack ice, *J. Geophys. Res.*, 92(C1), 779–782, doi:10.1029/JC092iC01p00779.
- Millero, F. J., C.-T. Chen, A. Bradshaw, and K. Schleicher (1980), A new high pressure equation of state for seawater, *Deep Sea Res., Part A*, 27(3–4), 255–264, doi:10.1016/0198-0149(80)90016-3.
- Morison, J., M. Steele, and R. Andersen (1998), Hydrography of the upper Arctic Ocean measured from the nuclear submarine U.S.S. Pargo, *Deep Sea Res., Part I*, 45(1), 15–38, doi:10.1016/S0967-0637(97)00025-3.
- Muench, R. D. (1990), A review of mesoscale processes in the polar oceans, in *Polar Oceanography*, edited by W. O. Smith, pp. 223–285, Academic, N. Y.
- Müller, P., J. C. McWilliams, and M. J. Molemaker (2005), Routes to dissipation in the ocean: The 2D/3D turbulence conundrum, in *Marine Turbulence*, edited by H. Z. Baumert, J. Simpson, and J. Sündermann, pp. 397–405, Cambridge Univ. Press, Cambridge, U. K.
- Nastrom, G. D., and K. S. Gage (1985), A climatology of atmospheric wavenumber spectra of wind and temperature observed by commercial aircraft, *J. Atmos. Sci.*, 42(9), 950–960, doi:10.1175/1520-0469(1985)042<0950:ACOAWS>2.0.CO;2.
- Nurser, A. J. G., and S. Bacon (2014), The Rossby radius in the Arctic Ocean, *Ocean Sci.*, 10(6), 967–975, doi:10.5194/os-10-967-2014.
- Padman, L. (1995), Small-scale physical processes in the Arctic Ocean, in *Arctic Oceanography: Marginal Ice Zones and Continental Shelves*, edited by W. O. Smith Jr., and J. M. Grebmeier, p. 288, AGU, Washington, D. C., doi:10.1029/CE049.
- Percival, D. B., and A. T. Walden (1993), *Spectral Analysis for Physical Applications*, Cambridge Univ. Press, Cambridge, U. K.
- Pinkel, R. (2005), Near-inertial wave propagation in the Western Arctic, *J. Phys. Oceanogr.*, 35(5), 645–665, doi:10.1175/jpo2715.1.
- Rainville, L., and P. Winsor (2008), Mixing across the Arctic Ocean: Microstructure observations during the Beringia 2005 Expedition, *Geophys. Res. Lett.*, 35, L08606, doi:10.1029/2008GL033532.
- Rainville, L., C. Lee, and R. Woodgate (2011), Impact of wind-driven mixing in the Arctic Ocean, *Oceanography*, 24(3), 136–145, doi:10.5670/oceanog.2011.65.
- Rudels, B. (2001), Arctic Basin circulation, in *Encyclopaedia of the Ocean Sciences*, edited by K. Turekian, J. H. Steele, and S. A. Thorpe, pp. 177–187, Academic, San Diego, Calif.
- Rudels, B., G. Björk, J. Nilsson, P. Winsor, I. Lake, and C. Nohr (2005), The interaction between waters from the Arctic Ocean and the Nordic Seas north of Fram Strait and along the East Greenland Current: Results from the Arctic Ocean-02 Oden expedition, *J. Mar. Syst.*, 55(1–2), 1–30, doi:10.1016/j.jmarsys.2004.06.008.
- Samelson, R. M., and C. A. Paulson (1988), Towed thermistor chain observations of fronts in the subtropical North Pacific, *J. Geophys. Res.*, 93(C3), 2237–2246, doi:10.1029/JC093iC03p02237.
- Serreze, M. C., and R. G. Barry (2011), Processes and impacts of Arctic amplification: A research synthesis, *Global Planet. Change*, 77(1–2), 85–96, doi:10.1016/j.gloplacha.2011.03.004.
- Shcherbina, A. Y., E. A. D'Asaro, C. M. Lee, J. M. Klymak, M. J. Molemaker, and J. C. McWilliams (2013), Statistics of vertical vorticity, divergence, and strain in a developed submesoscale turbulence field, *Geophys. Res. Lett.*, 40, 4706–4711, doi:10.1002/grl.50919.
- Steele, M., and T. Boyd (1998), Retreat of the cold halocline layer in the Arctic Ocean, *J. Geophys. Res.*, 103(C5), 10,419–10,435, doi:10.1029/98JC00580.
- Thorpe, S. A. (2007), *An Introduction to Ocean Turbulence*, Cambridge Univ. Press, Cambridge, U. K.

- Timmermans, M. L., and P. Winsor (2013), Scales of horizontal density structure in the Chukchi Sea surface layer, *Cont. Shelf Res.*, *52*, 39–45, doi:10.1016/j.csr.2012.10.015.
- Timmermans, M. L., S. Cole, and J. Toole (2012), Horizontal density structure and restratification of the Arctic Ocean surface layer, *J. Phys. Oceanogr.*, *42*(4), 659–668, doi:10.1175/jpo-d-11-0125.1.
- Tulloch, R., and K. S. Smith (2009), Quasigeostrophic turbulence with explicit surface dynamics: Application to the atmospheric energy spectrum, *J. Atmos. Sci.*, *66*(2), 450–467, doi:10.1175/2008JAS2653.1.
- Tulloch, R., J. Marshall, C. Hill, and K. S. Smith (2011), Scales, growth rates, and spectral fluxes of baroclinic instability in the ocean, *J. Phys. Oceanogr.*, *41*(6), 1057–1076, doi:10.1175/2011JPO4404.1.
- Van Zandt, T. E. (1982), A universal spectrum of buoyancy waves in the atmosphere, *Geophys. Res. Lett.*, *9*(5), 575–578, doi:10.1029/GL009i005p00575.
- Wadhams, P., and N. R. Davis (2000), Further evidence of ice thinning in the Arctic Ocean, *Geophys. Res. Lett.*, *27*(24), 3973–3975, doi:10.1029/2000GL011802.
- Wadhams, P., N. Hughes, and J. Rodrigues (2011), Arctic sea ice thickness characteristics in winter 2004 and 2007 from submarine sonar transects, *J. Geophys. Res.*, *116*, C00E02, doi:10.1029/2011JC006982.
- Wang, D.-P., C. N. Flagg, K. Donohue, and H. T. Rossby (2010), Wavenumber spectrum in the Gulf Stream from shipboard ADCP observations and comparison with altimetry measurements, *J. Phys. Oceanogr.*, *40*(4), 840–844, doi:10.1175/2009JPO4330.1.
- Wang, M., and J. E. Overland (2009), A sea ice free summer Arctic within 30 years?, *Geophys. Res. Lett.*, *36*, L07502, doi:10.1029/2009GL037820.